npg

ORIGINAL ARTICLE

Study on a 2D layer coordination framework showing order-to-disorder phase transition by ionothermal synthesis

Wenqian Chen[1], Satoshi Horike[1,2], Munehiro Inukai[3] and Susumu Kitagawa[1,3]

In this study, a two-dimensional (2D) layer-type coordination framework showing solid-to-solid phase transition was ionothermally synthesized. $[Zn_2(SO_4)_3(bpy)](THMA)_2$ contains an anionic 2D grid layer-type coordination framework and an ordered bulky ammonium cation, $THMA^+$, with multiple hydrogen bonds. The compound shows reversible order-to-disorder transformation, a result of the cations, which were characterized using X-ray diffraction, differential scanning calorimetry and solid state nuclear magnetic resonance. This study suggests the potential use of coordination frameworks, prepared by ionothermal synthesis, in the design of new type of materials that show solid-to-solid phase transition and high thermal stability for dielectric, ferroelectric and electro-optic functions.

INTRODUCTION

Solid-to-solid phase transition compounds with reversible structural changes have been of wide interest. For example, the phase transition associated with the reorientational order–disorder motion of molecules and ions in crystals are reported in organic and organic–inorganic hybrid chemistry.[1–3] Tuning and switching motions of molecular or ionic rotators with polarity in crystals correlate with dielectric, ferroelectric and electro-optic functions.[4] Coordination frameworks composed of metal ions and bridging ligands are promising candidates to construct such crystals because their structures can be tuned by the combination of rigid cavities and mobile guest molecules or ions.[5,6] Ammonium metal formate is one of a family of coordination frameworks that exhibit a reversible order–disorder transition via H-bond formation and breaking, and they show unique dielectric properties.[7–12] Many formate-based frameworks with transition metal ions have been studied; however, the synthesis strategy of other types of coordination frameworks that exhibit phase transition remains limited, despite their significant potential for electric functional materials.

In this study, we demonstrate the synthesis of a Zn^{2+} coordination framework showing clear solid-to-solid phase transition using ionothermal synthesis. Synthesis of crystalline compounds in ionic liquids, namely ionothermal synthesis, has been recently studied due to its unique properties and wide choice of ionic liquids.[13–16] A huge combination of ions can form ionic liquids. We are able to construct coordination frameworks with a variety of cations and anions from ionic liquids. The value of ionothermal synthesis for solid-to-solid phase transition in coordination frameworks is discussed.

EXPERIMENTAL PROCEDURE

All chemicals and deoxidized solvents in the synthesis were purchased from commercial vendors and used without further purification. All manipulations, unless otherwise stated, were performed under an Ar atmosphere in an Ar-filled glove box or using the standard Schlenk technique.

For the synthesis of $[Zn_2(SO_4)_3(bpy)](THMA)_2$ (1), $Zn(NO_3)_2 \cdot 4H_2O$ (0.2 mmol) and 4,4′-bipyridyl (bpy, 0.1 mmol) were dissolved in a mixture solution of $[THMA]^+[MeSO_4]^-$ (10 mmol) and dimethylformamide (26 mmol) under Ar atmosphere. The mixture was stored at 60 °C for 12 h and the colorless crystalline product 1 was formed. The crystals were filtered and washed with dimethylformamide (20 ml, three times) to remove the residual solvent and dried at 25 °C under Ar atmosphere for a day.

Single crystal X-ray diffraction measurements were performed under N_2 flow on a Rigaku AFC10 diffractometer, with a Rigaku Saturn Kappa CCD system incorporating a MicroMax-007 HF/VariMax (Kyoto, Japan) rotating-anode X-ray generator with confocal monochromated MoKα radiation. Data were processed by a direct method (SIR97) and refined by full-matrix least-squares method using the SHELXL-97 computer program (http://shelx.uni-ac.gwdg.de/SHELX/download.php). Thermogravimetry analysis was performed using a Rigaku TG8120 under flowing nitrogen employing a $10 \, \text{K} \, \text{min}^{-1}$ ramp rate. Crystal data of 1 and 1′ are shown in the Supporting information Supplementary Table S1. Sample preparations for thermogravimetry analysis were conducted under air. Differential scanning calorimetry (DSC) was performed with a Mettler Toledo DSC822e/200 instrument (Mettler-Toledo International, Inc, Im Langacher, Switzerland), at a heating rate of $10 \, \text{K} \, \text{min}^{-1}$.

[1]Department of Synthetic Chemistry and Biological Chemistry, Graduate School of Engineering, Kyoto University, Kyoto, Japan; [2]Japan Science and Technology Agency, PRESTO, Saitama, Japan and [3]Institute for Integrated Cell-Material Sciences (WPI-iCeMS), Kyoto University, Kyoto, Japan
Correspondence: Dr S Horike, Department of Synthetic Chemistry and Biological Chemistry, Kyoto University, Katsura, Nishikyo-ku, Kyoto 615-8510, Japan.
E-mail: horike@sbchem.kyoto-u.ac.jp
or Professor S Kitagawa, Institute for Integrated Cell-Material Sciences (WPI-iCeMS), Kyoto University, Yoshida, Sakyo-ku, Kyoto 606-8501, Japan
E-mail: kitagawa@icems.kyoto-u.ac.jp
Received 28 August 2014; revised 24 September 2014; accepted 8 October 2014; published online 12 November 2014

Sample preparations for DSC were conducted under Ar. X-ray powder diffraction data were collected on a Rigaku RINT 2200 Ultima diffractometer with CuKα anode. Solid state ^{13}C cross polarization magic angle spinning nuclear magnetic resonance spectra were recorded on a Bruker ADVANCE 400 MHz spectrometer (Bruker BioSpin Corp., Billerica, MA, USA); the spinning rate for cross polarization magic angle spinning spectra was 6 kHz for ^{13}C. Impedance analyses were performed as follows. Sample powders (~25–30 mg) were pressed at 500 kg N for 2 min and sandwiched between two platinum electrodes with a 5 mm diameter. Measurements were performed using an impedance and gain-phase analyser (Solartron SI 1260 impedance/gain-phase analyzer (Solartron Analytical, Hampshire, UK)) over a frequency range of 1–1 MHz, with an input voltage amplitude of 30 mV. Pellet preparation and impedance measurements were performed inside a glove box under Ar atmosphere. ZView software (Scribner Associates Inc., Southern Pines, NC, USA) was used to fit the impedance data sets by means of an equivalent circuit simulation to obtain the resistance values.

RESULTS AND DISCUSSION

A coordination crystal framework was synthesized from a $Zn(NO_3)_2 \cdot 6H_2O$, bpy and [THMA][$MeSO_4$]/dimethylformamide 1:1 (volume ratio) mixed solution at 60 °C. We obtained colorless crystals, denoted hereafter as 1. To investigate the crystal structure of 1, we measured its single crystal X-ray diffraction at −100 °C, as shown in Figure 1. The formula of 1 was [$Zn_2(SO_4)_3$(bpy)](THMA)$_2$. The $MeSO_4^{2-}$ anion changed to SO_4^{2-}, as indicated in the crystal structure analysis. The Zn^{2+} ions were coordinated to one N atom from the bpy ligand, and three O atoms from SO_4^{2-} ions to form a tetrahedral coordination geometry (Figure 1a). SO_4^{2-} anions connect two independent Zn^{2+} ions to form inorganic one-dimensional chains along the *c* axis, with each chain linked by the bpy ligand along the *b* axis to form a grid-type 2D layer structure, as shown in Figure 1b. The size of the grid was estimated to be 10×8 Å, and the 2D layers were stacked along the *a* axis. There was no proton in this layered structure and no specific interaction between the adjacent layers, such as hydrogen bond (H-bond) or pi–pi stacking.

For the charge balance, THMA$^+$ was intercalated in the 2D layers, as shown in Figure 1c. As THMA$^+$ has three hydroxyl groups, we observed multiple hydrogen bonds with the anionic coordination polymer [$Zn_2(SO_4)_3$(bpy)]$^{2-}$. There was one H-bond between two neighboring THMA$^+$ (Figure 1d), and seven H-bonds between THMA$^+$ and the anionic framework in the unit cell. The O···H–O hydrogen bond distance was in the 1.9–2.6 Å range and in the 2.8–3.0 Å range for the S···H–O hydrogen bond distance. These mutual H-bonds stabilize the overall structure of 1.

The crystals of 1 were deliquescent, and powder X-ray diffraction (PXRD) was used to measure a ground sample of the single crystal under Ar atmosphere, as shown in Figure 2a. The observed pattern corresponded to the simulated pattern from the single crystal X-ray study, indicating a successful synthesis of 1 with single phase and a large scale. Thermogravimetry analysis for 1 is shown in Figure 2b. Due to the high hydrophilicity of 1, it easily adsorbs water from the air; the thermogravimetry analysisprofile showed a 10% weight loss below 70 °C because the water attached to the crystal surface. No weight loss was observed until 200 °C, suggesting that 1 remains thermally stable until this temperature under N_2. We measured DSC of 1 from 25–200 °C under a N_2 atmosphere (Figure 2c). Interestingly, a sharp endothermic peak was observed at 115 °C in the heating process, and an exothermic peak at 100 °C in the cooling process. Three cycles of DSC in the temperature range of 25–200 °C were measured, with the peaks reversibly observed in each heating/cooling cycle. Calculated values of enthalpy for the first cycle were $\Delta H_{endo} = 32.5$ kJ mol^{-1} and $\Delta H_{exo} = -31.4$ kJ mol^{-1}, which will be discussed below. The morphology of the microcrystals of 1 was also monitored by microscope with heating under a Ar atmosphere, and no change was observed above the endothermic temperature (115 °C). This indicates that the endothermic behavior in the heating process would not occur due to the melting of 1, yet it suggests solid–solid phase transition.

To investigate the mechanism behind this thermal behavior of 1, we measured the temperature variable PXRD under a N_2 atmosphere. Figure 3 shows the powder patterns of heating (28–200 °C) and cooling (200–28 °C) processes. The initial crystal structure was retained until 110 °C, and the pattern changed at 130 °C in the heating process. We denote this form as 1′. The PXRD pattern of 1′ was observed in the temperature range of 130–200 °C in the heating process and from 200 °C to 120 °C in the cooling process. The pattern at 80 °C in the cooling process indicated that 1′ transformed to 1. The structural transformation from 1 to 1′ was crystal-to-crystal, with the transition temperatures corresponding to those observed in the DSC profile. Therefore, we concluded that the sharp endothermic and exothermic peaks in the DSC profile were a product of the reversible crystal structure transformation in the solid state.

To understand the structural transformation in detail, we conducted a single crystal X-ray diffraction for 1′. The crystal structure of 1, shown in Figure 1, was determined at −100 °C. To observe the crystal structure of 1′ above 115 °C, where the structural transformation occurs, we slowly heated the single crystal 1 to promote
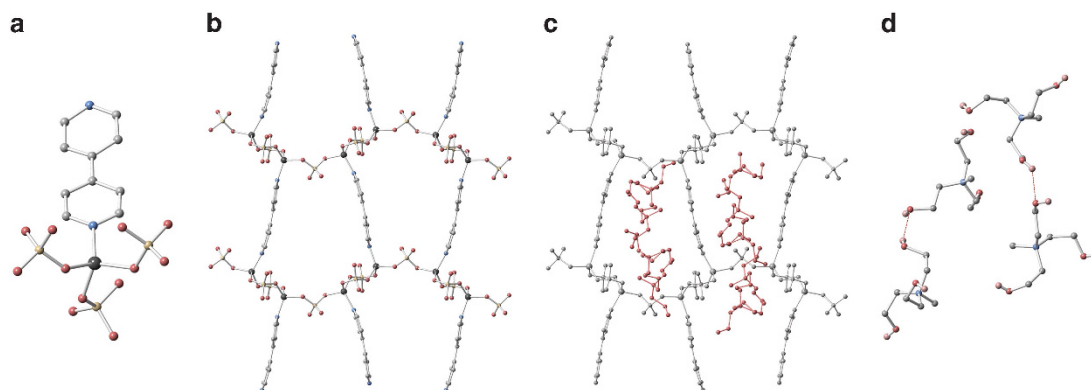

Figure 1 (**a**) Coordination environment around Zn^{2+} in 1. (**b**) Two-dimensional (2D) grid-type layer structure of 1. (**c**) 2D layer structure of 1 (gray: 2D layer, pink: THMA$^+$). (**d**) H-bond structure of two THMA$^+$ dimer in 1. Gray, blue, pink, yellow, pale pink and black are C, N, O, S, H and Zn, respectively. H atoms are omitted.
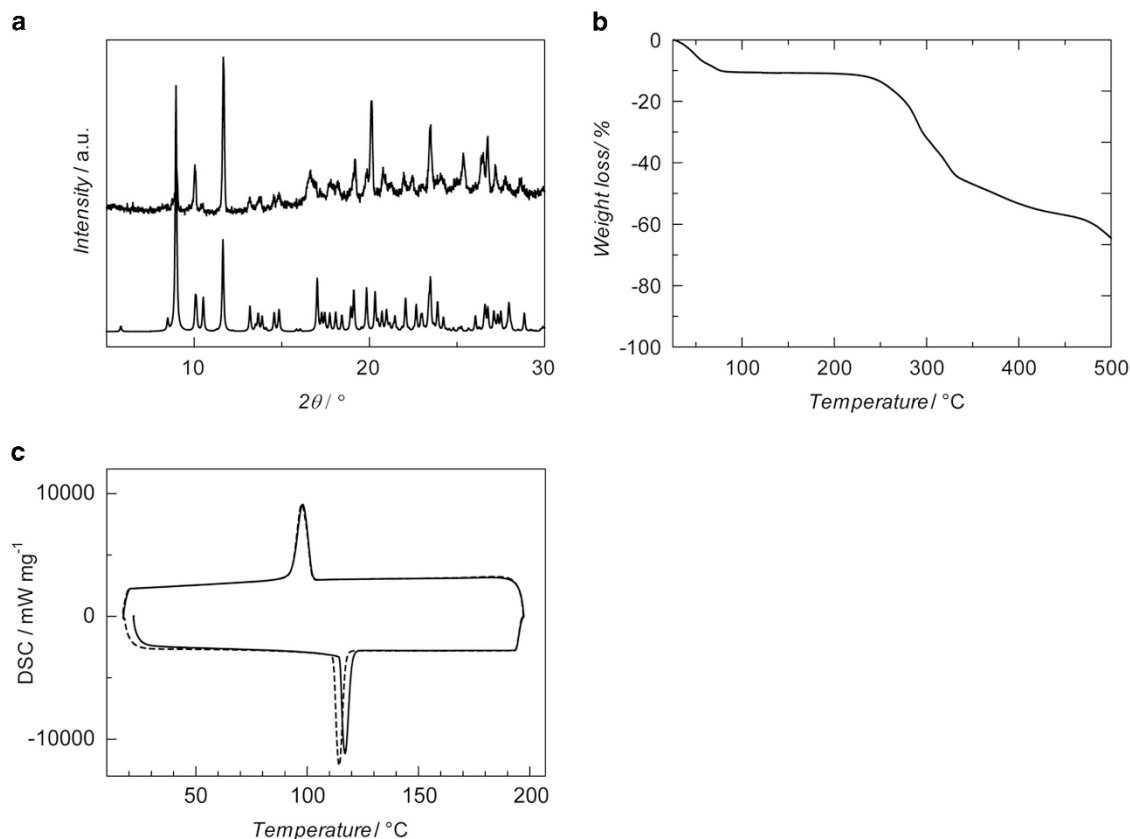
Figure 2 (**a**) Powder X-ray diffraction patterns of 1 under a N_2 atmosphere with the simulated pattern from single crystal analysis. (**b**) Thermogravimetry analysis profile of 1. (**c**) Differential scanning calorimetry profile of 1 under Ar atmosphere. Solid line represents the first cycle and the dotted line represents the second cycle of the heating/cooling process.
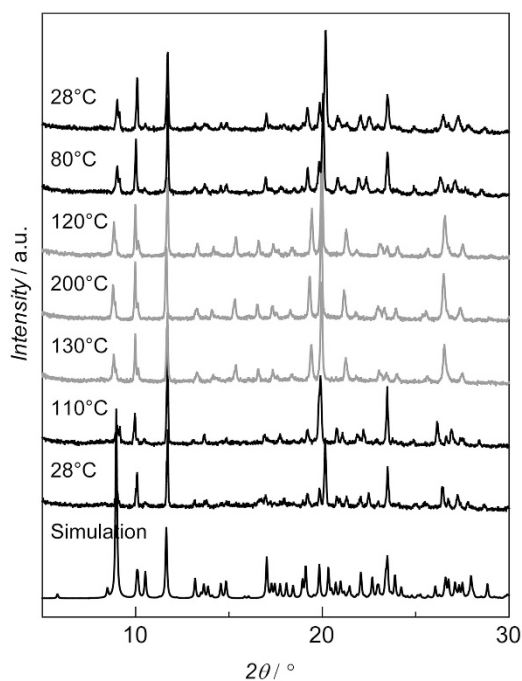

Figure 3 Temperature variable powder X-ray diffraction patterns with the simulated pattern of 1 under a N_2 atmosphere. Measurements were conducted from 28 °C (bottom) to 200 °C (middle) to 28 °C (upper). powder X-ray diffraction patterns with a gray color represent 1′ phase.

transformation and measured the diffraction of 1′ at 140 °C (Figure 4). For the crystal structure determined at this temperature the final R value was relatively large because of the heavy disorder. The structure of 1′ suggests that the grid-type 2D layer structure remained intact after the structural transformation. On the other hand, there were several differences in the structures of 1 and 1′. Cell parameters and the volume of 1′ were larger than those of 1, with a change also observed in the space group (1: monoclinic, 1′: orthorhombic). However, we could not observe $THMA^+$ in the structure of 1′, due to its disorder in this structure. The disorder of $THMA^+$ is induced by H-bond breaks, which resulted in the structural rearrangement for 2D grid coordination polymer. The disordered structure of 1′ was retained in the wide temperature region from 115 to 200 °C, indicating the high thermal stability in 1′.

We compared the PXRD patterns of 1′ and the simulated pattern from the single crystal X-ray analysis and found that the two were in good agreement (Supporting information Supplementary Figure S1). This supports the observation that the crystal structure corresponds to the high temperature phase 1′ studied from temperature variable PXRD and DSC. The sharp peaks in the DSC profile were predominantly attributed to the order-to-disorder transition of the accommodated $THMA^+$ in the 2D layer structure. The enthalpy of order–disorder from 1 to 1′ in the heating process was $\Delta H_{endo} = 32.5$ $kJ\,mol^{-1}$, based on DSC results. This value was much larger than that reported for ammonium metal formate frameworks whose ΔH_{endo} were less than $10\,kJ\,mol^{-1}$.[4,17–19] This is a result of $THMA^+$ being bulky and having a low symmetry, with multiple H-bond sites. By
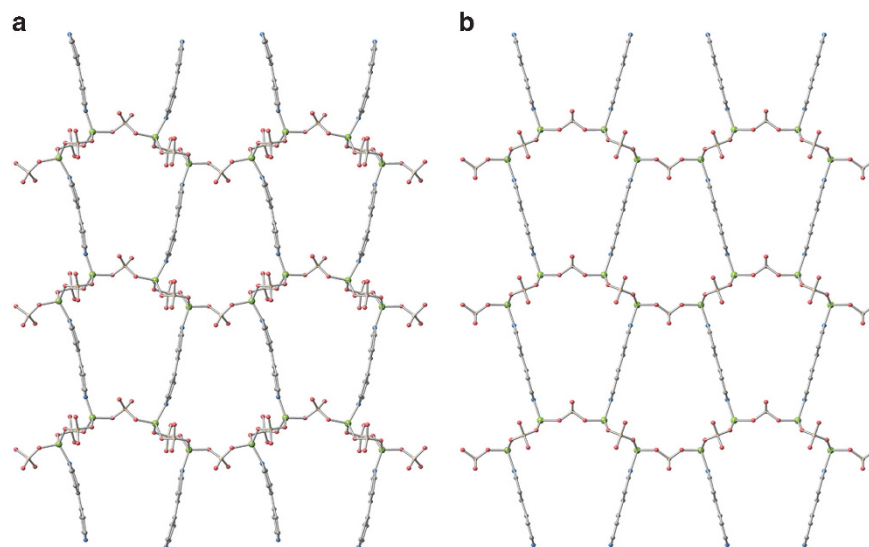
Figure 4 Crystal structures for the two-dimensional layer of $[Zn_2(SO_4)_3(bpy)]^{2-}$ for (**a**) 1 measured at $-100\,°C$ and (**b**) 1′ measured at $140\,°C$.

considering the Boltzmann equation $\Delta S = R\ln(N)$, where R is the gas constant and N is the ratio of the number of distinguishable states for different phases, we obtained $N > 10^4$, which indicates a completely isotropic rotation of THMA$^+$ in the cavity of 1′. As one THMA$^+$ has eight H-bonds, a single H-bond shares $4\,kJ\,mol^{-1}$ on average, which is a reasonable amount of energy for H-bond cleavage. Crystals with dynamic components in the structure are often categorized as plastic crystals.[20–22] Plastic crystals are defined as compounds that undergo a large-enthalpy-change phase transition from a solid-to-solid phase, and in the case of molecular ionic plastic crystals, an entropy change of $< 20\,J\,mol^{-1}\,K^{-1}$. For 1 to 1′, the entropy change at $115\,°C$ was larger than this because 1 has multiple H-bonds in the structure. As a result, the order–disorder transition was attributed to the cooperative breaks of H-bonds, and the disordered state of 1′ smoothly transforms to 1 at $95\,°C$.

To monitor the chemical environment and dynamics of $[Zn_2(SO_4)_3(bpy)]^{2-}$ and THMA$^+$ in 1 and 1′, we measured the solid state ^{13}C nuclear magnetic resonance under various temperatures (Figure 5). At $25\,°C$, three distinct peaks were observed at 125, 150 and 153 p.p.m., which were attributed to the bpy ligand. These peaks have a spinning side band, suggesting that the bpy are fixed in the 2D layer. Multiple peaks of THMA$^+$ at 50–70 p.p.m. were observed, which represents two crystallographically different cations. We did not observe a significant change of the spectrum at $70\,°C$; however, the peaks of THMA$^+$ became broader, bringing 1 closer to the phase transition of 1′. The ^{13}C nuclear magnetic resonance spectrum of 1′ at $137\,°C$ was obviously different from 1. All peaks were sharper than those in 1. More specifically the peaks for THMA$^+$ became isotropic, supporting the fast isotropic motion of THMA$^+$ in 1′. As a result of the isotropic motion, the two independent THMA$^+$ in 1 appear to be in a similar chemical environment in 1′. The spectrum of 1′ changes to 1 with cooling and the reversibility of 1 and 1′ was confirmed from the nuclear magnetic resonance spectra.

To study the dynamics of ionic components in 1 and 1′, we conducted impedance spectroscopy for a pelletalized sample of 1 under an Ar atmosphere. Figure 6 shows Nyquist plots of 1′ at $170\,°C$ and an Arrhenius plot as heating processed. The figure shows typical Nyquist plots attributed from ionic conduction for all temperatures. The observed conductivity was $7 \times 10^{-10}\,S\,cm^{-1}$ at $50\,°C$, whereas
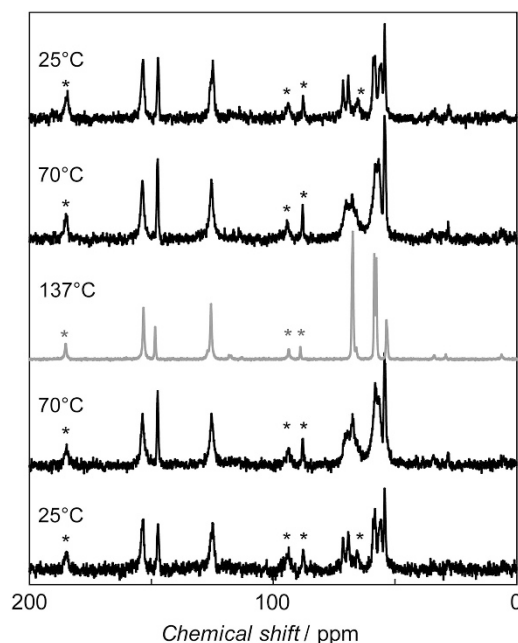

Figure 5 Temperature variable ^{13}C solid state cross polarization magic angle spinning nuclear magnetic resonance spectra of 1 (black) and 1′ (gray) from $25\,°C$ (bottom) to $137\,°C$ (middle) to $25\,°C$ (upper). The spinning rate was 6 kHz and spinning side bands are shown with an asterisk.

the conductivity was negligible for 1. The conductivity increased with the heat, reaching $2 \times 10^{-7}\,S\,cm^{-1}$ at $170\,°C$, where 1 had transformed to 1′. The Arrhenius plot was linear with no flexion point observed at the transition temperature from 1 to 1′ ($115\,°C$). This indicates that the ion conductivity was not related to the order-to-disorder transformation of THMA$^+$. On the other hand, the conductive ion species is likely to be the proton (H$^+$) in the hydroxyl groups of THMA$^+$ as the calculated activation energy of this conductivity was $0.6\,eV$, which is an appropriate value for H$^+$ conductivity.[23] As the two THMA$^+$ form dimers via interionic H-bonds in 1, there is no continuous H-bond network in the
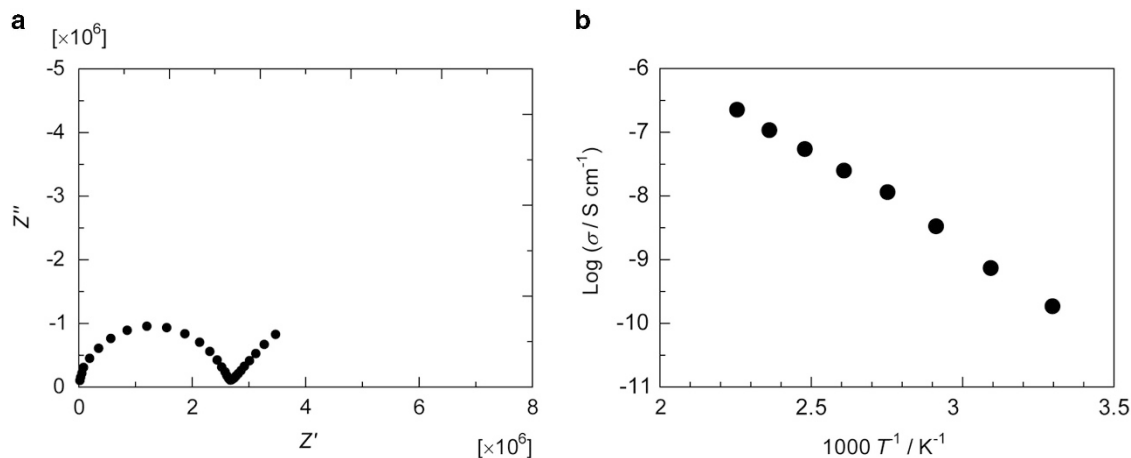
Figure 6 (a) Nyquist plot of 1′ at 170 °C under an Ar atmosphere. (b) Arrhenius plot of ion conductivity via structure transition from 1 to 1′ in the heating process.

alignment of the cations. This feature remains, even in 1′, as reversibility of this transition was observed; thus, the Arrhenius plot shows a linear profile. A detailed study of the dielectric property of 1 and 1′ will be the next step.

CONCLUSIONS

In conclusion, we demonstrated the synthesis of a Zn^{2+} 2D layer-type crystalline coordination framework, which shows a unique solid-to-solid transformation by ionothermal synthesis. Crystallographic analysis indicated that bulky ammonium cations derived from ionic liquid were fixed to the 2D layer coordination framework with multiple H-bonds and behaved completely isotropically above 115 °C with a breaking of the H-bonds. This order-to-disorder transformation was reversible, with the disorder state thermally stable until 200 °C. This result provides an interesting guideline for the synthesis of materials showing solid-to-solid phase transition based on the coordination framework.

ACKNOWLEDGEMENTS

1 Horiuchi, S., Ishii, F., Kumai, R., Okimoto, Y., Tachibana, H., Nagaosa, N., Tokura, Y. Ferroelectricity near room temperature in co-crystals of nonpolar organic molecules. *Nat. Mater.* **4**, 163–166 (2005).

2 Sun, Z., Chen, T., Luo, J., Hong, M. Bis(imidazolium) L-tartrate: a hydrogen-bonded displacive-type molecular ferroelectric material. *Angew. Chem. Int. Ed.* **51**, 3871–3876 (2012).

3 Pardo, E., Train, C., Liu, H., Chamoreau, L. M., Dkhil, B., Boubekeur, K., Lloret, F., Nakatani, K., Tokoro, H., Ohkoshi, S., Verdaguer, M. Multiferroics by rational design: implementing ferroelectricity in molecule-based magnets. *Angew. Chem. Int. Ed.* **51**, 8356–8360 (2012).

4 Zhu, Q., Shang, R., Chen, S., Liu, C., Wang, Z., Gao, S. [(C$_2$H$_5$)$_4$N][U$_2$O$_4$(HCOO)$_5$], an Ammonium Uranyl Formate Framework Showing Para- to Ferro-Electric Transition: Synthesis, Structures, and Properties. *Inorg. Chem.* **53**, 8708–8716 (2014).

5 Weng, D. F., Wang, Z. M., Gao, S. Framework-structured weak ferromagnets. *Chem. Soc. Rev.* **40**, 3157–3181 (2011).

6 Zhang, W., Xiong, R. G. Ferroelectric metal-organic frameworks. *Chem. Rev.* **112**, 1163–1195 (2012).

7 Jain, P., Dalal, N. S., Toby, B. H., Kroto, H. W., Cheetham, A. K. Order-disorder antiferroelectric phase transition in a hybrid inorganic-organic framework with the perovskite architecture. *J. Am. Chem. Soc.* **130**, 10450–10451 (2008).

8 Jain, P., Ramachandran, V., Clark, R. J., Zhou, H. D., Toby, B. H., Dalal, N. S., Kroto, H. W., Cheetham, A. K. Multiferroic behavior associated with an order-disorder hydrogen bonding transition in metal-organic frameworks (MOFs) with the perovskite ABX$_3$ architecture. *J. Am. Chem. Soc.* **131**, 13625–13627 (2009).

9 Sanchez-Andujar, M., Presedo, S., Yanez-Vilar, S., Castro-Garcia, S., Shamir, J., Senaris-Rodriguez, M. A. Characterization of the order-disorder dielectric transition in the hybrid organic-inorganic perovskite-like formate Mn(HCOO)$_3$[(CH$_3$)$_2$NH$_2$]. *Inorg. Chem.* **49**, 1510–1516 (2010).

10 Xu, G. C., Ma, X. M., Zhang, L., Wang, Z. M., Gao, S. Disorder-order ferroelectric transition in the metal formate framework of [NH$_4$][Zn(HCOO)$_3$]. *J. Am. Chem. Soc.* **132**, 9588–9590 (2010).

11 Li, M., Liu, B., Wang, B., Wang, Z., Gao, S., Kurmoo, M. Erbium-formate frameworks templated by diammonium cations: syntheses, structures, structural transition and magnetic properties. *Dalton Trans.* **40**, 6038–6046 (2011).

12 Stroppa, A., Barone, P., Jain, P., Perez-Mato, J. M., Picozzi, S. Hybrid improper ferroelectricity in a multiferroic and magnetoelectric metal-organic framework. *Adv. Mater.* **25**, 2284–2290 (2013).

13 Cooper, E. R., Andrew, C. D., Wheatley, P. S., Webb, P. B., Wormald, P., Morris, R. E. Ionic liquids and eutectic mixtures as solvent and template in synthesis of zeolite analogues. *Nature* **430**, 1012–1016 (2004).

14 Parnham, E. R., Morris, R. E. Ionothermal synthesis of zeolites, metal-organic frameworks, and inorganic-organic hybrids. *Acc. Chem. Res.* **40**, 1005–1013 (2007).

15 Aidoudi, F. H., Aldous, D. W., Goff, R. J., Slawin, A. M., Attfield, J. P., Morris, R. E., Lightfoot, P. An ionothermally prepared S = 1/2 vanadium oxyfluoride kagome lattice. *Nat. Chem.* **3**, 801–806 (2011).

16 Freudenmann, D., Wolf, S., Wolff, M., Feldmann, C. Ionic liquids: new perspectives for inorganic synthesis? *Angew. Chem. Int. Ed.* **50**, 11050–11060 (2011).

17 Tang, Y., Ji, C., Sun, Z., Zhang, S., Chen, T., Luo, J. Phase Transition Originating from Order-Disorder Transformations of Carboxy Oxygen Atoms Coupled with Dynamic Proton Motions in [PhCH$_2$NH(CH$_3$)$_2$]$_2$C$_2$O$_4$H$_2$C$_2$O$_4$. *Chem. Asian J.* **9**, 1771–1776 (2014).

18 Shang, R., Xu, G. C., Wang, Z. M., Gao, S. Phase transitions, prominent dielectric anomalies, and negative thermal expansion in three high thermally stable ammonium magnesium-formate frameworks. *Chem. Eur. J.* **20**, 1146–1158 (2014).

19 Maczka, M., Pietraszko, A., Macalik, B., Hermanowicz, K. Structure, phonon properties, and order-disorder transition in the metal formate framework of [NH$_4$][Mg(HCOO)$_3$]. *Inorg. Chem.* **53**, 787–794 (2014).

20 Timmermans, J. Plastic crystals: A historical review. *J. Phys. Chem. Solids* **18**, 1–8 (1961).

21 MacFarlane, D. R., Forsyth, M. Plastic Crystal Electrolyte Materials: New Perspectives on Solid State Ionics. *Adv. Mater.* **13**, 957–966 (2001).

22 Pringle, J. M., Howlett, P. C., MacFarlane, D. R., Forsyth, M. Organic ionic plastic crystals: recent advances. *J. Mater. Chem.* **20**, 2056 (2010).

23 Kreuer, K.-D. Proton Conductivity: Materials and Applications. *Chem. Mater.* **8**, 610–641 (1996).

Supplementary Information accompanies the paper on Polymer Journal website (http://www.nature.com/pj)